Reprinted from The Journal of Physical Chemistry, 1993, 97.


# Damage to $CF_3CONH$-Terminated Organic Self-Assembled Monolayers (SAMs) on Al, Ti, Cu, and Au by Al K$\alpha$ X-rays Is Due Principally to Electrons

**Robert L. Graham, Colin D. Bain,† Hans A. Biebuyck, Paul E. Laibinis, and George M. Whitesides***

*Department of Chemistry, Harvard University, Cambridge, Massachusetts 02138*

*Received: April 14, 1993; In Final Form: June 16, 1993*•

This paper models damage induced by monochromatized Al K$\alpha$ X-rays to organic thin films using self-assembled monolayers supported on Al, Ti, Cu, and Au. An X-ray photoelectron spectrometer is used both to conduct the X-ray irradiation and to analyze the damage. In all cases these monolayers comprised a trifluoroacetimido ($CF_3CONH$–) group bound to the substrate through an undecyl tether to either a chemisorbed thiolate or carboxylate. This work extends a previous study of using trifluoroacetoxy-terminated SAMs on Au and Si. We find the X-ray-induced damage to the $CF_3CONH$-terminated SAM is first order in the loss of fluorine. From a comparative study of the loss of fluorine from monolayers formed on these substrates with different electron yields, we show directly that electrons, not X-rays, are the principal cause of damage to the monolayer films. These results are relevant to the design of new materials targeted to fabrication at small dimensions by X-ray or electron lithography.

## Introduction

Understanding the molecular mechanisms of the damage to organic materials that occur on exposure to X-rays is useful in controlling the resulting changes in their properties[1-3] and in designing materials for use in technologies such as X-ray lithography.[4-6] In this paper, we describe the use of organic self-assembled monolayers (SAMs) as model systems to study X-ray-induced damage using monochromatized Al K$\alpha$ X-ray radiation ($E$ = 1486.6 eV, $\lambda$ = 8.34 Å).[7,8] We use an X-ray photoelectron spectrometer both to conduct the X-ray irradiation and to analyze the damage. This use of the spectrometer both as an X-ray generator for inducing the damage, and as an analytical tool, is particularly convenient experimentally and introduces no artifacts in manipulating or transferring the sample between X-ray irradiation and analysis. SAMs are well suited for this study because they are structurally well-defined and have dimensions (10–40-Å thickness perpendicular to the plane of the monolayer) that are of the same order as the inelastic scattering length (the escape depth) for electrons induced by these soft X-rays—≤15 keV—of 20–40 Å.[9]

The objectives of this study were (i) to design a system with which to investigate the kinetics of damage, (ii) to form structurally-related SAMs on a variety of substrates that exhibit different electron yields on X-ray irradiation, in order to explore the hypothesis that photoinduced electrons, not X-ray photons, are the principal source of damage[10] in these monolayer systems,[7,8] and (iii) to provide an upper bound to the importance of the X-rays (relative to the X-ray-induced photoelectrons) in the damage observed. The conclusions from these studies—that the X-ray-induced primary and secondary electrons[11] are the predominant species responsible for the damage in the organic film—suggest that to decrease the damage for a given X-ray dose, it is necessary to reduce the yield of photoelectrons from the substrate. This conclusion also suggests that in the design of new materials involving organic films having nanometer thicknesses for use in X-ray[5,6] and electron lithography,[12,13] it is possible to base the design on the hypothesis that both types of lithography result from the same molecular mechanism for damage: the interaction of electrons with the organic film.

X-ray damage has previously been studied in polymer systems. Polyvinylchloride loses chlorine readily on irradiation with X-rays[14,15] in a process that was presumed to be induced directly by photoionization. Mihaly and Zuppiroli investigated X-ray damage to organic conductors[16] and suggested that the level of damage scaled with the total absorbed energy (an observation that is consistent with electrons as the principal cause of damage). Pepper studied the degradation of perfluoro polyethers (PFPE) using a monochromatized Al K$\alpha$ source and degradation of poly(tetrafluoroethylene) (PTFE) using a nonmonochromatized Mg K$\alpha$ source;[17] Chaney and Barth studied PTFE using a monochromatized Al K$\alpha$ source.[18] Both studies reported extensive rearrangement, cross-linking, and fragmentation of the polymer. Storp reviewed radiation damage in organic films by electron and X-ray beams and concluded that the available evidence did not establish whether the primary agent of damage was the X-ray photons, emitted by the X-ray sources or electrons photoejected from within the samples.[19] In a recent communication, we described the use of trifluoroacetoxy-terminated SAMs on systems consisting of a gold film (used to generate electrons) separated from the SAM by a silicon layer (to scatter photoelectrons ejected from the gold).[8] We concluded that electrons generated in the substrates were the principal cause of X-ray-induced damage.

The study of X-ray-induced damage using an experimental system comprising SAMs and monochromatic Al K$\alpha$ radiation has several advantages. The molecular-level structures of SAMs can be controlled with high precision, and their structures have been characterized by a large number of techniques, including IR spectroscopy,[20] STM,[21] He,[22] electron,[23] grazing-angle X-ray diffraction,[24,25] wetting, and ellipsometry.[26,27] SAMs allow a variety of organic functionalities to be incorporated;[27] in these studies, we use trifluoroacetyl-terminated SAMs. Figure 1 shows a schematic illustration of the structures used in these studies. We chose the $CF_3CONH$ group because its surface concentration is easily measured by XPS, it decomposes rapidly when irradiated with X-rays, it is localized at the monolayer–air interface so that analysis of the concentration of F is not complicated by the presence or generation of other signals (as with the damage of PTFE). All the samples used in this study are conducting and do not require use of a compensating electron flood gun to maintain charge neutrality during X-ray irradiation. In the monochromatized XPS spectrometer we used to irradiate the samples and to monitor damage, there are only two plausible causes of damage: direct X-ray-induced processes, or inelastic scattering

† Present address: Physical Chemistry Laboratory, South Parks Rd., Oxford OX13QZ, UK.

* To whom correspondence should be addressed.

• Abstract published in *Advance ACS Abstracts*, August 15, 1993.

0022-3654/93/2097-9456$04.00/0 

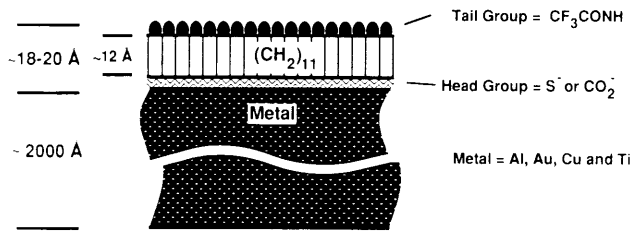


**Figure 1.** Schematic illustration of the structures used in these studies. The metal films of Al, Au, Cu, and Ti (~2000 Å in thickness) are supported on Si wafers primed with an adhesion layer of Cr or Ti (~100 Å in thickness, not shown). The Si and the adhesion layer in the supports are separated from the organic self-assembled monolayer (SAM) by thicknesses of the metal which are ≳50× the escape depth of electrons through the metal film; thus, the supports do not influence the observed damage to the SAMs. The SAMs (~18–20 Å in thickness) that are formed on each metal film have a head group covalently attached to the metal, a common length tether of $(CH_2)_{11}$ (~12 Å in thickness), and a $CF_3$ tail group at the monolayer–vacuum interface. At the metal–head group interface of the Al, Cu, and Ti systems is an oxide (not shown) of undetermined thickness (but probably ~15 Å). The cant angle of the backbone of the polymethylene chain from the normal to the surface of the substrate varies from 30° (for thiolates on gold) to ≈10° (for thiolates on copper).

of the electrons that arise from the interaction of the X-rays with the sample. Stray electrons from the X-ray anode are attenuated by a 4-μm Mylar window between the X-ray anode and monochromator. The use of a Mylar window significantly reduces the generation of any measurable secondary electrons at the sample and further isolates the sample from the effect of heating from the X-ray source.[10,28,29]

In this study, we investigated the initial kinetics for the loss of fluorine from the $CF_3CONH$ group in a self-assembled monolayer of $CF_3CONH(CH_2)_{11}SH$ on Au. The kinetics observed are consistent with a first-order loss of fluorine from the SAM. We also investigate whether electrons are the principal cause of damage for SAMs formed on a broader class of metal substrates (Al, Ti, and Cu), extending our earlier work,[8] which examined trifluoroacetoxy-terminated monolayers on Au and Si. The X-ray-induced electrons have a different energy distribution from substrates of Au, Cu, Ti, and Al. The results indicate that when the probability of an inelastic collision of the electrons with the monolayer is considered, the electrons and not the X-rays are principally responsible for the observed damage. We show that damage in the SAM induced directly by the absorption of X-ray photons and photoionization can account for at most 5–10% of the observed loss of fluorine.

## Results and Discussion

**Substrate Preparation.** In the study of the initial kinetics for the loss of fluorine from the SAM, we used gold substrates thermally evaporated on chromium-primed silicon wafers. The advantages of using gold substrates with alkanethiol-derived SAMs are (i) the substrates can be handled in ambient conditions in the laboratory and (ii) by patterning the gold on the silicon wafer, we can control the spatial formation of the SAMs (since thiols do not adsorb on $SiO_2$[30]). To study whether the X-rays or electrons generated in the substrates are the principal cause of the damage observed, we required metals with a range of photogenerated electron yields on which we could adsorb $CF_3$-CONH-terminated SAMs. Gold, silver, and copper, in addition, are the reference standards for XPS adopted by the ASTM and are therefore well characterized.[10,31] The gold and copper substrates have a relatively high photogenerated electron yield compared to the $Al/Al_2O_3$ or $Ti/TiO_2$ substrates.[32]

**Preparation of Monolayers.** The surfaces were derivatized by the self-assembly technique. Alkanethiols were used to react with soft metal–metal oxides of gold and copper. SAMs were formed by the adsorption of alkanoic acids on $Al/Al_2O_3$ or $Ti/TiO_2$. The details of the monolayer preparation are given in the Experimental Section.

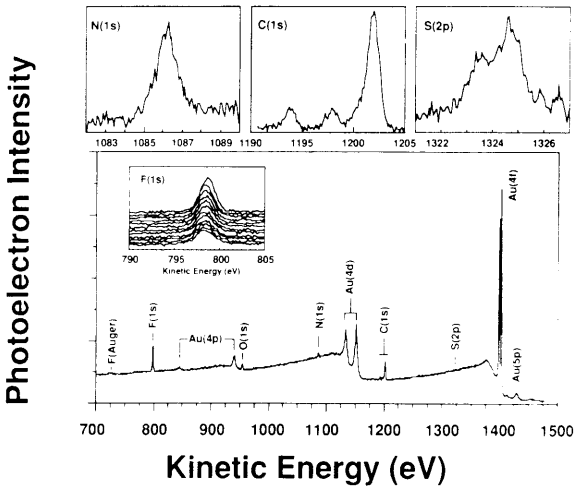


**Figure 2.** XPS survey spectrum of an $Au/S(CH_2)_{11}NHCOCF_3$ SAM system. High resolution XPS spectra of the S(2p), C(1s), and N(1s) regions, indicated in the survey spectrum, are also shown of the SAM on gold. The inset shows high resolution spectra of the F(1s) region of $Au/S(CH_2)_{11}NHCOCF_3$ system upon prolonged exposure to X-rays. Time progresses from the top to the bottom with sequential spectra taken at intervals of 1 h. The last spectrum corresponds to 11 h of exposure to the Al Kα X-ray source.

**Characterization of Monolayers.** We used X-ray photoelectron spectroscopy (XPS) with a monochromatic Al Kα X-ray source (1486.6 eV) for characterization of the monolayer and as our principal diagnostic tool to follow the damage in these $CF_3CONH$-terminated self-assembled monolayers. Figure 2 shows an XPS survey spectrum of the $Au/S(CH_2)_{11}NHCOCF_3$ SAM system. High-resolution spectra for N(1s), C(1s), and S(2p) confirm the composition of the SAM. Detailed assignments are given in the Experimental Section. The inset shows high-resolution spectra of the F(1s) region of the XPS spectra on prolonged exposure of the SAM to Al Kα X-rays (for a total of 11 h). The shift in the position of the F(1s) peak energy to lower kinetic energy is significant and reproducible. The shifts observed in the peak position of the F(1s) peak probably arise from changes in the polarizability of the monolayers and not changes in the chemical state of the fluorine.[33] A similar trend is observed in SAMs formed from mixtures of $HS(CH_2)_2(CF_2)_9CF_3$ and $HS(CH_2)_{10}$-$CH_3$:[34] the kinetic energy of the F(1s) peak decreases with decreasing mole fraction of $HF(CH_2)_2(CF_2)_9CF_3$ in the SAM.

**Analysis of the Kinetics of the Loss of Fluorine from $Au/S(CH_2)_{11}NHCOCF_3$ on X-ray Irradiation: The Influence of the Shape of the X-ray Beam Profile.** The normalized loss of fluorine from the self-assembled monolayers for a first-order process with an X-ray beam with uniform intensity is given by an exponential decay:

$$I_{F(1s)}^{uniform}(t)/I_{F(1s),t=0} = e^{-at} \qquad (1)$$

where $I_{F(1s)}^{uniform}(t)$ is the intensity of the F(1s) peaks determined by XPS at time $t$, $I_{F(1s),t=0}$ is the initial F(1s) intensity and $a$ is the exponential damage constant. For our experimental conditions, however, the X-ray spatial profile is not uniform. We expect a normalized loss of fluorine that decays more slowly than the exponential form (eq 1) due to the smaller intensity of X-rays in the tails of the spatial profile compared to the central area of the beam. As a second model to compare to the observed loss of fluorine, we consider the case of a Gaussian spatial profile.[35] In Appendix I, we derive an expression for the normalized first-order loss of fluorine for the case of an X-ray beam having a Gaussian spatial profile:

$$I_{F(1s)}^{Gaussian}(t)/I_{F(1s),t=0} = (1 - e^{-bt})/bt \qquad (2)$$

where $I_{F(1s)}^{Gaussian}(t)$ is the intensity of the F(1s) peaks determined by XPS at time $t$, $I_{F(1s),t=0}$ is the initial F(1s) intensity and $b$ is a constant characterizing the damage.

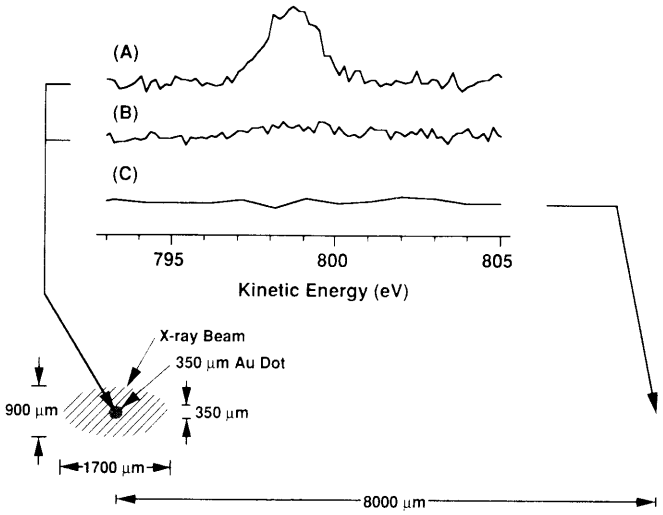


**Figure 3.** Schematic illustration showing the top view of the X-ray-induced damage experiment on a monolayer of $HS(CH_2)_{11}NHCOCF_3$ self-assembled on a 350-$\mu$m-diameter dot of Au. The size of the lithographically prepared Au dot was verified with an optical microscope. The SAM was positioned at the center of the X-ray beam (with the dimensions of 900 $\mu$m × 1700 $\mu$m as shown) to investigate the effect of the X-ray spatial intensity on the loss of fluorine observed from the SAM. XPS spectra of the F(1s) region taken at the center of the dot are shown (**A**) at the beginning of the damage experiment and (**B**) after 16.6 h of X-ray-induced damage has occurred. The F(1s) region is also shown (**C**) for a position on the sample 8000 $\mu$m from the center of the Au dot at the beginning of the damage experiment to verify that the monolayer forms only where Au has been evaporated.

To investigate the influence of the shape of the beam profile on the kinetics of the loss of fluorine, we compared two types of samples: (i) a sample with Au uniform over the wafer and (ii) a sample in which the SAM was supported on a gold "dot" having a diameter comparable to that of the X-ray beam. For the first, we derivatized a gold-coated chromium-primed silicon wafer with $HS(CH_2)_{11}NHCOCF_3$ by self-assembly from ethanol (see Figure 1). For the second, we prepared 350-$\mu$m gold dots by evaporation through a mask onto a silicon wafer. These dots were also derivatized with the trifluoroacetamido-terminated alkanethiol using the same procedure. The thiol does not adsorb to the silicon dioxide surface of the wafer in the absence of gold.[30,36]

Figure 3 shows a schematic of the X-ray-induced damage experiment using the 350-$\mu$m dot of Au derivatized with $HS(CH_2)_{11}NHCOCF_3$. The X-ray beam used in these experiments is projected from the monochromator on the sample as an ellipse with a semiminor diameter of 900 $\mu$m and a semimajor diameter of 1700 $\mu$m[28] (Figure 3). Figure 4 shows a scanning electron micrograph of the damage region of the SAM on a gold-coated wafer (bright region in the micrograph).[37,38] This image confirms the dimensions of the region exposed to X-rays shown in the schematic (Figure 3) and shows that this region of damage is inhomogeneous (as a result of the nonuniform spatial profile of the X-ray beam). A high-resolution scan of the F(1s) region taken at the center of the Au dot is shown in Figure 3 at the beginning of the damage experiment (**A**) and after a 16.6-h exposure to the X-ray beam (**B**) when 80% of the initial F has been lost from the monolayer. As a control, we also examined the F(1s) spectrum in a region centered 8000 $\mu$m from the dot of Au (**C**). The absence of any F in this region confirms that there is no formation of SAM on the $Si/SiO_2$.[30,36]

Figure 5 shows the normalized intensity of the F(1s) peak (plotted on a logarithmic scale) for the X-ray-induced damage of the $Au/S(CH_2)_{11}NHCOCF_3$ system compared with the Au[350-$\mu$m dot]/$S(CH_2)_{11}NHCOCF_3$ system versus time. The first-order loss of fluorine on irradiation with X-rays with a uniform spatial profile would follow a straight line in this figure (shown for each system as the dashed line, given by eq 1). The figure also compares these two systems with a first-order loss of fluorine for the case of a Gaussian X-ray beam profile. A least-squares fit for the loss of 20% of the fluorine was used to calculate the initial damage rate constant, $k$, for both systems (Table I). The first-order loss of fluorine for the case of the Gaussian X-ray beam profile (shown for each system as the solid line, given by eq 2) was determined by fitting the constant $b$ (eq 2) to the observed initial loss of fluorine for each system.[39]

Both the $Au/S(CH_2)_{11}NHCOCF_3$ and Au[350-$\mu$m dot]/$S(CH_2)_{11}NHCOCF_3$ systems show a loss of fluorine that is slower than the exponential form (eq 1). This observation suggests that there is a spatial variation in the intensity of the X-ray beam across the sample. Given the signal-to-noise ratio (especially for the Au[350-$\mu$m dot]/$S(CH_2)_{11}NHCOCF_3$ system), both systems are fit adequately by the first-order Gaussian spatial profile model

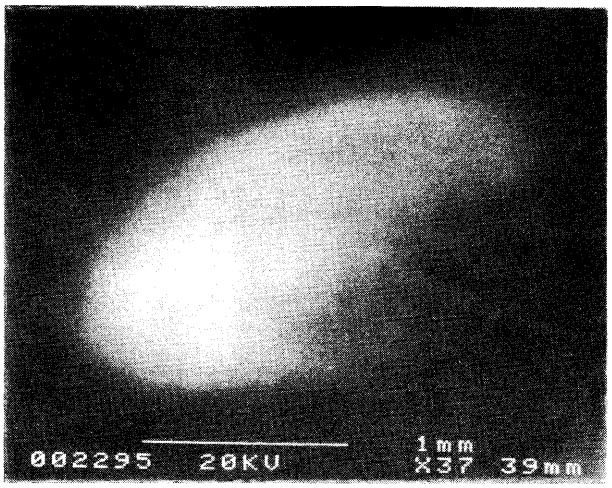


**Figure 4.** Scanning electron micrograph of the damage region for a gold coated Si wafer that had been derivatized with $HS(CH_2)_{11}NHCOCF_3$ and exposed to 12 h of X-ray irradiation. The light region is that part of the film that has been damaged.

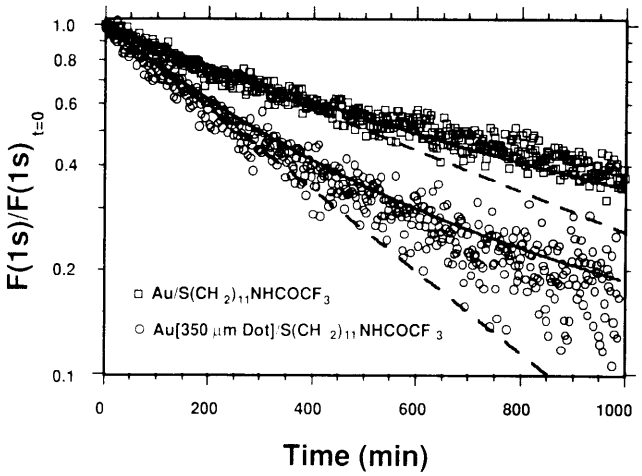


**Figure 5.** X-ray-induced damage to $HS(CH_2)_{11}NHCOCF_3$ monolayers assembled on an Au coated wafer ($Au/S(CH_2)_{11}NHCOCF_3$) and a 350-$\mu$m-diameter dot of Au (Au[350-$\mu$m dot]/$S(CH_2)_{11}NHCOCF_3$) as described in Figure 3. The normalized intensity of the F(1s) signal was determined from sequential scans, each lasting 2 min. Fits of the data are shown for first-order kinetic processes with two different models of the X-ray spatial profile. The model for a *uniform* X-ray spatial profile (simple exponential) is drawn as a dashed line (straight lines on this log plot) (eq 1). The model for a *Gaussian* X-ray spatial profile is drawn as a solid line (eq 2).

**TABLE I: Initial Damage Rates, $k$, for Au/$S(CH_2)_{11}NHCOCF_3$ and [350-$\mu$m dot Au]/$S(CH_2)_{11}NHCOCF_3$[a]**

| system | $10^5k$, $s^{-1}$ |
|---|---|
| $Au/S(CH_2)_{11}NHCOCF_3$ | 2.2 |
| [350-$\mu$m dot Au]$S(CH_2)_{11}NHCOCF_3$ | 4.4 |

[a] $k$ is determined by a least squares fit to $1 - kt$ using a loss of 20% of the F(1s) intensity as measured by XPS for both systems.

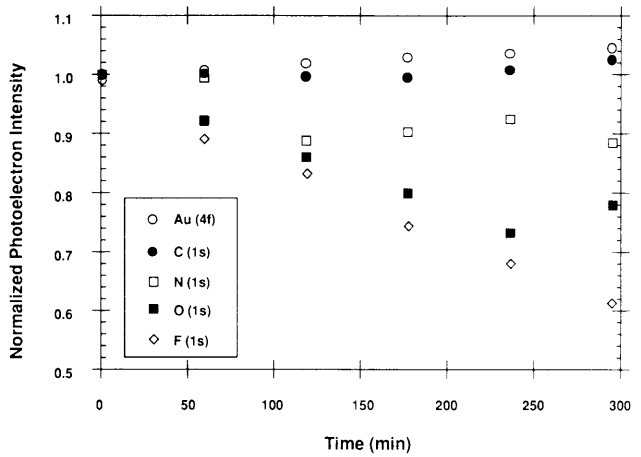


**Figure 6.** Normalized photoelectron intensities of the Au(4f), C(1s), N(1s), O(1s), and F(1s) from $Au/S(CH_2)_{11}NHCOCF_3$ on exposure to X-rays.

(eq 2) to the normalized loss of fluorine observed. The Au-[350-$\mu$m dot]/$S(CH_2)_{11}NHCOCF_3$ system has twice the initial loss of fluorine compared to the $Au/S(CH_2)_{11}NHCOCF_3$ system. The relative rates of damage are consistent with a model in which the SAM on the 350-$\mu$m dot of Au experiences a higher X-ray intensity per area compared to the unrestricted $Au/S(CH_2)_{11}NHCOCF_3$ system since the dot of Au is restricted to the central region of the nonuniform X-ray beam. The loss of fluorine from the dot is therefore faster than the rate of loss of fluorine from the $Au/S(CH_2)_{11}NHCOCF_3$ system.

**Where in the SAM Is the Damage Occurring? Loss of Other Elements from the Monolayer on Irradiation with X-rays.** Using XPS we can determine which elements are lost from the SAM during the exposure to X-ray irradiation. Loss of the F(1s) signal does not imply loss of the entire absorbate. Figure 6 compares the loss of some of the constituents of the trifluoroacetamido-terminated SAMs on Au. For these SAMs, the relative rates of loss are: $F \approx O > N > C$. It is unclear at what point (or points) of attachment the cleavage is occurring to result in the loss of fluorine; however, most of the damage occurs in the vicinity of the $-CF_3$ group, and the similarity in the rates of loss of F and O suggest that fragments involving $CF_3CO$ may be lost as a unit at least part of the time. The decrease in the attenuation of the Au(4f) intensity indicates that the thickness of the monolayer decreases $\sim$1 Å after 5 h (Figure 6) and 3 ± 2 Å after 16 h of exposure to X-rays in our experiment. These results suggest that the damage is confined to the region of the monolayer–vacuum interface. Other workers have observed that the components of SAMs supported on Si and Ag that have been irradiated using a synchrotron X-ray source remain largely intact.[24,25] In our case, we have not established the basis for the localization of damage in the region close to the SAM–vacuum interface. There are at least three possibilities: (i) it may simply reflect the fact that the $NHCOCF_3$ is located in this region and that this group damages more rapidly than $(CH_2)_n$ groups; (ii) damage deeper in the SAM may tend to be less likely to result in loss of material (either because of recombination of radical intermediates or because the fragments are trapped by non-covalent interactions); (iii) some fraction of damage may reflect the reaction of the SAM with species generated in the vapor phase (for example, oxygen and nitrogen atoms or ions generated by electron impact with background amounts of $O_2$, $H_2O$, and $N_2$).

**Investigation of the Physical Mechanism of X-ray Damage to Self-Assembled Monolayers on Metal Substrates: Is the Damage Caused Principally by the X-rays or by Electrons from the Substrates?** To address this question, we prepared trifluoracetamido-terminated self-assembled monolayers on substrates of Al, Ti, Cu, and Au. The $CF_3CONH-$ groups were attached to the substrates by a common undecyl tether $(CH_2)_{11}-$ to each substrate. The systems we used in this investigation were $Al/Al_2O_3/^-O_2C(CH_2)_{11}NHCOCF_3$,[40] $Ti/TiO_2/^-O_2C(CH_2)_{11}NHCOCF_3$, $Cu/S(CH_2)_{11}NHCOCF_3$,[41] and $Au/S(CH_2)_{11}NHCOCF_3$. Since each of these substrates is conducting, these systems could be analyzed by XPS without the use of a compensating electron flood gun. If the loss of fluorine occurs principally through direct X-ray-induced processes, then the rate of loss of fluorine from each substrate when exposed to a common flux of X-rays should be the same. If electrons—either primary photoelectrons or Auger electrons in the substrate or secondary electrons resulting from inelastic collisions of the primary electrons with the substrate or monolayer—are the principal cause of damage to the SAM, then fluorine will be lost more rapidly from the monolayers on substrates with the higher electron yields.

Figure 7A shows the XPS survey spectra of these derivatized substrates. The apparent intensities from the F(1s) peak from the $CF_3CONH-$ groups of the SAMs on the various substrates are not quantitatively comparable in these survey spectra. High-resolution spectra, shown in Figure 7B, of the F(1s) region indicate that the formation of the SAMs on the systems generated approximately equal numbers of $CF_3CONH-$ groups per unit area of surface.[42] The shifts observed in the peak position of the F(1s) on the four systems are probably arising from changes in the polarizability of the monolayers and not from electrical charging of the system from electron emission.[33,34]

The samples were exposed to a constant flux of monochromatized Al K$\alpha$ X-rays. Figure 8 summarizes the relative intensity of the F(1s) peak on the various substrates when exposed to X-rays. The intensity of the F(1s) peak for each system was measured at sequential intervals, each lasting 2 min. The amount of loss of fluorine from the various substrates exposed to common numbers of photons is different (Figure 8A). The loss of fluorine is faster on substrates that exhibit greater intensities of primary and secondary electrons on irradiation with X-rays (Figure 7A).

We use Figure 7A to estimate the relative importance of the photons and electrons in causing the damage to the SAMs. By summing the XPS survey spectra in Figure 7A over the measured electron energy range of 1486–130 eV, we estimated the yield of electrons using the $Au/S(CH_2)_{11}NHCOCF_3$ system as the reference standard. Although we were unable to measure below 130 eV, it is important to note that at these lower kinetic energies the electron intensities of the gold and copper SAM systems, for example, are systematically the same. The total relative electron yield, $Y_e$, is given by

$$Y_e = \sum_{KE=130\,eV}^{1487} J(KE)\,G(KE) \Big/ \left( \sum_{KE=130\,eV}^{1487} J(KE)\,G(KE) \right)_{Au} \quad (3)$$

where $J(KE)$ is the number of primary and secondary electrons[43] at kinetic energy, KE, and $G(KE)$ is a correction for the acceptance angle measured on the sample and the electron transmission efficiency of the hemispherical analyzer.[10,44,45] The subscript "Au" refers to the sum for the $Au/S(CH_2)_{11}NHCOCF_3$ system. Using the relative electron yield for each substrate, we plot (Figure 8B) the normalized loss of F(1s) from the four substrates versus the number of electrons to which the SAM was exposed.

The more physically relevant measure of damage to the film is the number of electrons scattered in the SAM not just number of electrons arriving at the detector. The probability of scattering an electron in the SAM depends on the kinetic energy, KE, of this electron and is expressed by the inelastic mean free path, $\lambda(KE)$, shown in Figure 9.[9,46] Substrates used in this study differ in both the number and *distribution* of their electrons (Figure 7A) so we can test effects due to scattering of electrons in the film.

Since the damage observed is confined to the monolayer-vacuum region of thickness $\delta(3 \pm 2$ Å), we use a Beer's law analysis (Appendix II) to determine at a given kinetic energy, KE, the

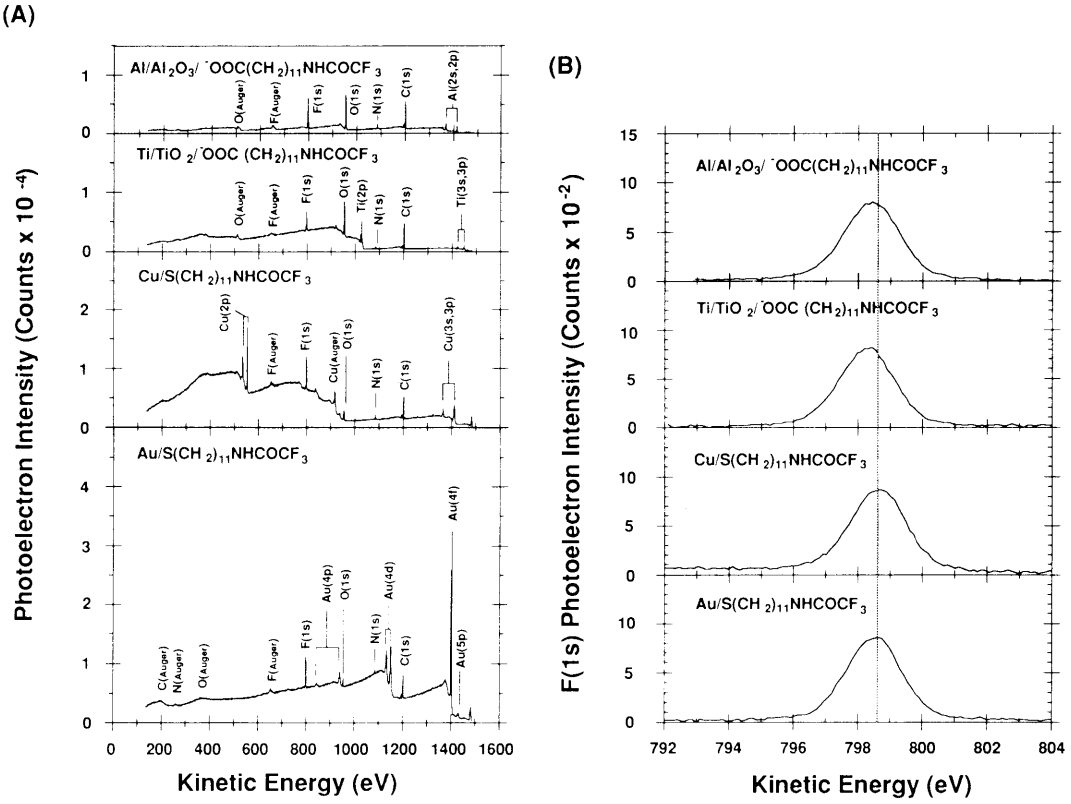


**Figure 7.** XPS survey spectra (**A**) of $Al/Al_2O_3/^-O_2C(CH_2)_{11}NHCOCF_3$, $Ti/TiO_2/^-O_2C(CH_2)_{11}NHCOCF_3$, $Cu/S(CH_2)_{11}NHCOCF_3$, and $Au/S(CH_2)_{11}NHCOCF_3$. The spectra have been stacked vertically, and are shown on the same scale of intensities to facilitate direct comparison. The XPS spectra were obtained on regions of the surface that had not been previously exposed to X-ray beam. The spectra required ~30 min of exposure to the beam; the amount of damage to the SAM during this exposure is small (<10%). The apparent intensities of the F(1s) region of the spectra are misleading in the survey spectra. High-resolution spectra (**B**) of the F(1s) region are shown for direct comparison.

number of inelastic electron collisions, $N_e^{inelas}(KE)$, in this layer relative to the $Au/S(CH_2)_{11}NHCOCF_3$ system as

$$N_e^{inelas}(KE) = \frac{\delta J(KE)\, G(KE)/\lambda(KE)}{(\delta J(KE)\, G(KE)/\lambda(KE))_{Au}} \quad (4)$$

Since the damage region, $\delta$, near the monolayer–vacuum interface for the $CF_3CONH$-terminated monolayers on each substrate should be the same, we can simplify this expression as

$$N_e^{inelas}(KE) = \frac{J(KE)\, G(KE)/\lambda(KE)}{(J(KE)\, G(KE)/\lambda(KE))_{Au}} \quad (5)$$

Hence, the weighted sum over all measured kinetic energies for the number of inelastically scattered electrons in these SAMs relative to the $Au/S(CH_2)_{11}NHCOCF_3$ system is

$$N_e^{inelas} = \frac{\sum_{KE=130\,eV}^{1487} J(KE)\, G(KE)/\lambda(KE)}{\left(\sum_{KE=130\,eV}^{1487} J(KE)\, G(KE)/\lambda(KE)\right)_{Au}} \quad (6)$$

In Figure 8C, we plot the relative intensity of the F(1s) peak from the various substrates versus the number of electrons inelastically depositing energy in the SAM as determined using the relative weights from (eq 6). With this correction for the inelastic scattering probability, all the profiles remain similar. We believe that the deviations present are due to difficulties in maintaining a constant photon flux. These data are consistent with the finding that electrons scattered by the film are principally responsible for the damage in these self-assembled monolayers upon irradiation with X-rays.

Table II compares for each of the four systems the total electron yield (eq 3) and the number of electrons inelastically scattered in the SAMs (eq 6) relative to the $Au/S(CH_2)_{11}NHCOCF_3$ reference system. Weighting of the electron yield by the inelastic mean free path (eq 6) explains why the $CF_3CONH$ groups in a SAM on Cu damage to the same level of loss of fluorine as those in a SAM on Au for the same number of photons (Figure 8A): the $CF_3CONH$ groups on both Au and Cu are exposed to the same relative number of electrons inelastically depositing energy in the SAM. This result stresses the significance of the use of the electron inelastic mean free path to correct for the likelihood of an electron with a given kinetic energy to interact with the SAM. When the relative electron distribution from the substrate is similar to Au (as with Si,[8] Al, and Ti) this correction is small, and using the electron yield (eq 3) gives a good estimate of the damage to the SAM (Figure 8B). When the electron distribution from the substrate is different from Au (as with Cu), correcting for the number of electrons inelastically scattered in the SAM is necessary to account for the observed loss of fluorine.

**What Direct Role Do X-rays Have in the Damage Mechanism of the Self-Assembled Monolayer Films?** Having demonstrated that the primary and secondary electrons are responsible for most of the damage to the organic films upon irradiation with X-rays, we wanted to establish an upper bound for the direct role that the X-ray photons have in the observed damage process. The SSX-100 XPS, operating at 200 W with an electron gun accelerating voltage of 10 keV, has $1.3 \times 10^{17}$ electrons striking the anode per second. The efficiency for the production of Al K$\alpha$,$\beta$ X-rays[47] is $22 \times 10^{-5}$ so the number of Al K$\alpha$,$\beta$ X-ray photons produced is $2.8 \times 10^{13}$ (s steradian)$^{-1}$. The reflection efficiency of the monochromator for Al K$\alpha$ radiation is 0.045[29] and the percentage of Al K$\alpha$ intensity is 88%[29] of the total K$\alpha$,$\beta$ X-ray photons emitted from the anode. With an angle subtended at the anode by the monochromator of 0.032 steradian[29] and the area of the X-ray spot (as shown in Figure 3) of 1.2 mm$^2$, the X-ray flux is $2.8 \times 10^{12}$ photons/(cm$^2$ s).

The total photoionization cross section of the $-NHCOCF_3$ group is $3 \times 10^5$ barns.[32] The probability at this X-ray flux of a photoionization event occurring in a given trifluoracetamido group is $8 \times 10^{-7}$ s$^{-1}$. If every photoionization event in the

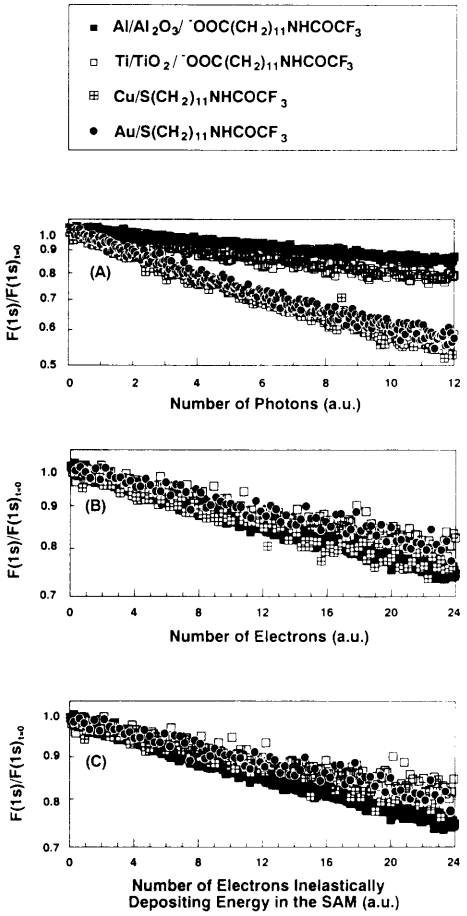


**Figure 8.** X-ray-induced damage to $Al/Al_2O_3/^-O_2C^-CH_2)_{11}NHCOCF_3$, $Ti/TiO_2/^-O_2C(CH_2)_{11}NHCOCF_3$, $Cu/S(CH_2)_{11}NHCOCF_3$, and $Au/S(CH_2)_{11}NHCOCF_3$ as a function of (**A**) the number of photons, (**B**) the number of electrons, and (**C**) the number of electrons inelastically depositing energy to the SAM. The intensity of the F(1s) peak was determined from sequential scans, each lasting 2 min (au, arbitrary units). We estimated the number of electrons from these samples by integrating the XPS survey spectra in Figure 7A and applying a correction for the detector efficiency of the instrument. The number of electrons inelastically depositing energy in the SAM was determined by weighting the XPS survey spectra in Figure 7A at each energy by the probability of an inelastic scattering event in the SAM based on the electron inelastic mean free path shown in Figure 9.

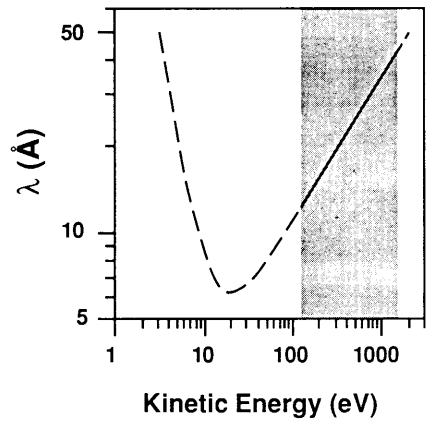


**Figure 9.** Inelastic mean-free path, λ, for an electron in hydrocarbon films vs kinetic energy. The inelastic mean free path is defined as the distance at which the probability of an electron transversing a medium without significant energy loss is 1/e. The shaded region shows the inelastic mean free path in the kinetic energy range measured by XPS. The solid curve is taken from a fit to the measured inelastic mean free path of monolayers of *n*-alkanethiols adsorbed on Cu, Ag, and Au,[46] and the dotted line is from Seah and Dench.[9]

$-NHCOCF_3$ group leads to the loss of all three fluorine atoms, then an upper limit for the rate of loss of fluorine atoms due to *direct* X-ray excitation of $2.8 \times 10^{12}$ photons/(cm$^2$ s) is

$$k^{\text{init}}_{\text{X-ray}}[F] = 2 \times 10^{-6}\ s^{-1}$$

Since the observed rate of loss of fluorine (in Table I) for the $CF_3CONH$-terminated monolayers on Au at this flux of X-ray photons is between $2 \times 10^{-5}$ and $4 \times 10^{-5}$ s$^{-1}$, the *direct* X-ray induced fluorine loss could account for no more than 5–10% of the damage observed.

**TABLE II: Comparison Relative to the Au/$S(CH_2)_{11}NHCOCF_3$ System of the Total Electron Yield, $Y_e$, and the Number of Electrons Inelastically Scattered in the SAM, $N_e^{\text{inelas}}$, As Measured by XPS**

| system | $Y_e$ | $N_e^{\text{inelas}}$ |
|---|---|---|
| $Al/Al_2O_3/^-O_2C(CH_2)_{11}NHCOCF_3$ | 0.16 | 0.16 |
| $Ti/TiO_2/^-O_2C(CH_2)_{11}NHCOCF_3$ | 0.38 | 0.43 |
| $Cu/S(CH_2)_{11}NHCOCF_3$ | 0.82 | 1.00 |
| $Au/S(CH_2)_{11}NHCOCF_3$ | 1.00 | 1.00 |

## Conclusions

X-ray-induced damage to $CF_3CONH$-terminated self-assembled monolayers is first order in the loss of fluorine. We have observed a strong correlation between the rate of damage and the number of electrons from the substrate of the organic monolayers. We estimate that the X-ray photons can only account for 5–10% of the observed fluorine loss; this estimate further reinforces the conclusion that the electrons, not the photons, are the principal damaging species. These results suggest that the design of new materials to be fabricated at small dimensions by either X-ray or electron lithography should be guided to give optimized results for damage occurring by the same physical process—the interaction of electrons with the organic film.

## Experimental Section

**Materials.** All chemicals were obtained from Aldrich and used as received unless specified otherwise. Previous work has described the preparation of 11-mercaptoundecanol.[20] We obtained 11-bromo-1-undecene from Pfaltz & Bauer, and hydrazine was obtained from Kodak. Isooctane and hexadecane were percolated twice through neutral alumina (EM Science) to remove polar impurities. Absolute ethanol (Quantum Chemical Corp.) and isooctane were deoxygenated with bubbling $N_2$ for 30 min prior to use. Single-crystal silicon (100) test wafers (100 mm diameter and ~0.5 mm thick) were obtained from Silicon Sense (Nashua, NH). Gold (99.999%) was obtained from Materials Research Corp. (Orangeburg, NY). Chromium (>99.99%), copper (99.99%), silver (99.9999%), and aluminum wire (99.99%) were all obtained from Aldrich. Elemental analyses were performed by Oneida Research Services. Melting points are reported uncorrected.

**Substrate and Monolayer Preparation.** Gold substrates were prepared by electron-beam evaporation of ~2000 Å of gold onto single-crystal silicon (100) wafers that had been precoated with 100–200 Å of chromium or titanium as an adhesion promotion layer between the silicon dioxide and the gold. The pressure in the cryopumped evaporator at the start of the evaporation was $1.6 \times 10^{-7}$ Torr. STM performed on gold substrates prepared by this procedure show crystallites of gold approximately 70 Å across and 20–30 Å high.[48]

To prepare the gold "dots", a mask was fabricated from brass shim stock (Precision Brand Products, Downers Grove, IL), ~150 μm thick, using an Easco Model 916 electric discharge machine with a 100-μm tungsten wire as the anode. The resulting holes were 190 ± 10 μm in diameter, as determined using an optical microscope. The mask was clamped over the silicon wafer to the evaporator stage through which chromium and gold were

evaporated as described above. The resulting Au dots had a diameter of 350 ± 10 μm.

Substrates for the copper monolayers were prepared analogously to the gold substrates with an ~100-Å titanium adhesion layer between the silicon oxide and the metal (thickness ~2000 Å). Aluminum substrates were prepared by electron-beam evaporation of ~1800 Å of Al onto the silicon wafers with a 100 Å titanium adhesion layer; the titanium substrates were prepared by electron-beam evaporation of ~1800 Å of Ti onto the silicon wafers.

**$Au/S(CH_2)_{11}NHCOCF_3$.** The gold slides, described above, were cut into ~1 cm × 3 cm slides with a diamond-tipped stylus, rinsed with ethanol, and blown dry in a stream of nitrogen. Adsorptions of $HS(CH_2)_{11}NHCOCF_3$ were carried out in 25-mL glass weighing bottles that had been cleaned with "piranha solution" (7:3 concentrated $H_2SO_4$/30% $H_2O_2$) at 90 °C for 1 h and rinsed first with distilled water and then with copious amounts of deionized water. **Warning**: Pirahna solution should be handled with caution. It should not be allowed to contact significant quantities of oxidizable organic materials. In some circumstances (most probably when mixed with significant quantities of an oxidizable organic material) it has detonated unexpectedly.[49] Weighing bottles were stored in an oven at ~200 °C until use. The adsorptions were performed for 1 day at room temperature using degassed absolute ethanol as the solvent.

**$Cu/S(CH_2)_{11}NHCOCF_3$.** The monolayers were prepared by a related procedure used for $Au/S(CH_2)_{11}NHCOCF_3$ except that the freshly evaporated Cu surfaces were transferred to the adsorbate solution under an inert atmosphere of flowing argon.[41] This procedure minimized exposure of the unfunctionalized Cu films to air.

**$Al/Al_2O_3/^-O_2C(CH_2)_{11}NHCOCF_3$ and $Ti/TiO_2/^-O_2C(CH_2)_{11}NHCOCF_3$.** Adsorptions of $CF_3CONH(CH_2)_{11}COOH$ were performed in 1 mM solution in isooctane as previously described.[40]

**Characterization of Monolayers.** XPS spectra of the SAMs exhibited only peaks due to the individual elements that comprised the adsorbate and those for the support metal. The C(1s) spectral envelope contains peaks that could be assigned to $(CH_2)_n$ [1202.0 eV], C=O [1198.0 eV], and $CF_3$ [1193.9 eV] (see, for example, the C(1s) spectrum in Figure 2).

**X-ray Photoelectron Spectrometer (XPS).** XPS spectra were acquired on a Surface Science Instruments X-100 spectrometer[29] equipped with an Al Kα source ($E$ = 1486.6 eV) and quartz monochromator operating with a background pressure in the range $10^{-8}$–$10^{-9}$ Torr. Detection is performed with a concentric hemispherical analyzer operating in fixed analyzer transmission mode, and multichannel detector with the angle between the sample and detector at 35°. No compensating flood gun was used in this study since all samples were conducting and grounded to the spectrometer. The spectra are referenced to C(1s) at 1202.0 eV. Survey spectra were acquired with a pass energy of 150 eV, an anode power of 200 W, and an elliptical X-ray beam with a semiminor diameter of 900 μm and a semimajor diameter of 1700 μm.

**Studies of Damage Induced by X-rays.** The damage profiles were acquired using the depth profile software provided with the XPS spectrometer. Unless otherwise stated, all spectra of the F(1s) peak were taken using a 15-eV window from kinetic energy 792–807 eV, a detector pass energy of 100 eV, and an X-ray spot size of 1000 μm (with actual dimensions on the sample of 900 μm × 1700 μm, as shown in Figure 4).

To study the loss of fluorine from the trifluoroacetamido-terminated monolayers in the kinetic investigation shown in Figure 5, the F(1s) region was scanned continuously with each scan lasting 2 min for 16.6 h for both the $Au/S(CH_2)_{11}NHCOCF_3$ and Au[350-μm Dot]/$-S(CH_2)_{11}NHCOCF_3$ system. We used a pass energy of 100 eV and a window of 15 eV.

For the comparative study of the loss of fluorine from the trifluoroacetamido-terminated monolayers (shown in Figure 8), the F(1s) region was scanned continuously with each scan lasting 2 min. The $Au/S(CH_2)_{11}NHCOCF_3$ system was run alternating as a control to monitor anode drift. The survey spectra (Figure 7A) were acquired with a pass energy of 100 eV in the kinetic energy range of 1486–130 eV. The lower kinetic energy limit was determined by the combined bias on the hemispherical analyzer (pass energy) and the detector entrance lens (~11 eV).

**Scanning Electron Microscopy.** The scanning electron micrograph in Figure 4 was taken on a JEOL JSM-6400 scanning electron microscope with an accelerating voltage of 20 keV and background pressure in the range $10^{-6}$ Torr.

**12-(Trifluoroacetamido)dodecanoic Acid.** Trifluoroacetic anhydride (1 mL) and triethylamine (1 mL) were added sequentially to 12-aminododecananoic acid (540 mg, 2.51 mmol) in 30 mL of $CH_2Cl_2$, and the mixture was stirred for 1 h. The solution was washed with distilled $H_2O$ (3 × 30 mL) and concentrated under vacuum to give a white solid. Recrystallization from hexane/$Et_2O$ gave 433 mg (1.39 mmol, 55.4%) of the title compound. $^1H$ NMR (250 MHz, $CDCl_3$) δ 6.29 (br s, 1 H), 3.34 (q, 2 H, $J$ = 6.6 Hz), 2.42 (t, 2 H, $J$ = 7.4 Hz), 2.33 (t, 2 H, $J$ = 7.4 Hz), 1.61 (m, 4 H) 1.2-1.4 (m, 12 H). Anal. Calcd (Found) for $C_{14}H_{24}F_3NO_3$: C, 54.01 (53.66); H, 7.77 (7.54); N, 4.50 (4.58); F, 18.31 (18.42).

**11-Phthalimido-1-undecene.** A solution of 11-bromo-1-undecene (11.5 g, 49.4 mmol), potassium phthalimide (10.2 g, 55.1 mmol), and DMF (100 mL) was refluxed for 4 h. After cooling to room temperature, 300 mL of distilled $H_2O$ was added. The product was obtained by extraction with hexanes (3 × 75 mL) and purified by recrystallization from EtOH to give the title compound as a white solid (13.3 g, 44.6 mmol, 90%). $^1H$ NMR (250 MHz, $CDCl_3$) δ 7.82 (m, 2 H), 7.69 (m, 2H), 5.79 (m, 1 H), 4.94 (d, 1 H, $J$ = 30 Hz), 4.92 (m, 1H), 3.65 (t, 2 H, $J$ = 7 Hz), 2.00 (quart, 2 H, $J$ = 7 Hz), 1.62 (m, 2 H, $J$ = 7 Hz), 1.2–1.4 (m, 12 H).

**11-Amino-1-undecene.** Hydrazine (7 mL) was added to a stirred solution of 11-phthalimido-1-undecene (30.2 g, 101 mmol) in 75 mL of absolute EtOH. After ~15 min, a white precipitate of phthalhydrazide formed. The solid was removed by filtration and the filtrate was concentrated under reduced pressure. The title compound (10.7 g, 63.1 mmol, 63%) was obtained as a colorless liquid by vacuum distillation (80–85 °C/≤0.5 mmol Hg,[50] 175–178 °C/10 mm). $^1H$ NMR (250 MHz, $CDCl_3$) δ 5.79 (m, 1 H), 4.94 (d, 1 H, $J$ = 29 Hz), 4.93 (m, 1 H), 2.66 (t, 2 H, $J$ = 7 Hz), 2.01 (q, 2 H, $J$ = 7 Hz), 1.61 (m, 2 H), 1.2–1.4 (m, 12 H).

**11-(Trifluoroacetamido)-1-undecene.** Trifluoroacetic anhydride (1.60 g, 7.61 mmol) was added dropwise to a solution of 11-amino-1-undecene (901 mg, 5.32 mmol) in 20 mL of $CH_2Cl_2$. Pyridine (1 mL) was then added. The solution was stirred for 2 h and subsequently concentrated. The title compound (1.31 g, 4.92 mmol, 92%) was obtained by chromatography (silica) using 3:1 hexanes/$CH_2Cl_2$ as eluant. $^1H$ NMR (300 MHz, $CDCl_3$) δ 6.25 (br s, 1 H), 5.79 (m, 1 H), 4.95 (d, 1 H, $J$ = 32 Hz), 4.94 (m, 1 H), 3.34 (quart, 2 H, $J$ = 7 Hz), 2.02 (quart, 2 H, $J$ = 7 Hz), 1.56 (m, 2 H, $J$ = 7 Hz), 1.2–1.4 (m, 12 H).

**11-(Trifluoroacetamido)-1-undecanethioacetate.** A solution of 11-(trifluoroacetamido)-1-undecene (1.31 g, 4.92 mmol), thioacetic acid (2 mL), and AIBN (10 mg) in 40 mL of THF was photolyzed for 15 h using a medium-pressure Hg lamp. The solution was concentrated, and the title compound obtained by chromatography (silica) using 30% $CH_2Cl_2$/hexanes. The product was further purified by recrystallization from hexanes yielding fine white needles (1.26 g, 3.68 mmol, 75%), mp 51.5–53.5 °C. $^1H$ NMR (250 MHz, $CDCl_3$) δ 6.26 (br s, 1 H), 3.34 (q, 2 H, $J$ = 7 Hz), 2.84 (t, 2 H, $J$ = 7 Hz), 2.30 (s, 3 H), 1.4–1.6 (m, 4 H), 1.2–1.4 (m, 10 H). Anal. Calcd (Found) for $C_{15}H_{26}F_3NO_2S$: C, 52.77 (52.82); H, 7.68 (7.74); N, 4.10 (4.02); F, 16.69 (16.53); S, 9.39 (9.60).

**11-(Trifluoroacetamido)-1-undecanethiol.** A methanolic solution (40 mL) of 11-(trifluoroacetamido)-1-undecanethioacetate (1.24 g, 3.62 mmol) was purged with $N_2$ for 2 h. Concentrated

HCl (2 mL) was added, and the solution was refluxed for 3 h under $N_2$. The solution was concentrated, and the title compound obtained as a white solid (734 mg, 2.45 mmol, 67%) by chromatography (silica) using 20% $CH_2Cl_2$/hexanes, mp 36.5–38.0 °C. $^1H$ NMR (250 MHz, $CDCl_3$) $\delta$ 6.24 (br s, 1 H), 3.34 (q, 2 H, $J$ = 7 Hz), 2.53 (q, 2 H, $J$ = 7 Hz), 1.4–1.6 (m, 2 H), 1.31 (t, 1 H, $J$ = 7 Hz), 1.2–1.4 (m, 10 H). Anal. Calcd (Found) for $C_{13}H_{24}F_3NOS$: C, 52.15 (52.34); H, 8.08 (8.37); N, 4.68 (4.66); F, 19.04 (18.50); S, 10.71 (11.12).

**Acknowledgment.** Supported in part by the Office of Naval Research, the Defense Advanced Research Projects Agency, and the National Science Foundation (grant no. CHE-88-12709 and DMR-89-20490). The X-ray photoelectron spectrometer (XPS) is an instrumental facility purchased under the DARPA/URI program and maintained by the Harvard University Materials Research Laboratory [MRL] (DMR-89-20490). The SEM and EDM were purchased and maintained by the Harvard MRL program. We thank J. L. Bell for help in preparing the mask by EDM, J. P. Folkers for assisting with the preparation of substrates, and J. R. Martin for discussions and suggestions.

## Appendix I. The Effect of a Nonuniform X-ray Spatial Intensity Profile on a First-Order Mechanism for Damage to the Self-Assembled Monolayer (SAM): The Case of a Gaussian Profile

From an X-ray source with a beam of uniform intensity, the expected loss of F from $Au/S(CH_2)_{11}NHCOCF_3$ for a first-order damage mechanism would have a simple exponential form:

$$I_{F(1s)}^{uniform}(t)/I_{F(1s),t=0} = e^{-at} \tag{I.1}$$

where $I_{F(1s)}^{uniform}(t)$ is the intensity of the F(1s) peaks determined by XPS at time $t$, $I_{F(1s),t=0}$ is the initial F(1s) intensity, and $a$ is the exponential damage constant.

An observed deviation from this familiar form, however, does not mean the damage mechanism is not a first-order process. If the X-ray source has a nonuniform spatial intensity profile, the loss of F from the SAM will not follow a simple exponential. For the case of a Gaussian X-ray intensity spatial profile, a closed form expression for the decay law is easily obtained.

Given a Gaussian X-ray beam intensity profile

$$I^x(r) = I_0^x e^{-r^2/2\sigma^2} \tag{I.2}$$

where $I_0^x$ is the amplitude of the X-ray beam intensity and $\sigma$ is the standard deviation of the spatial profile, the resulting intensity of electrons ejected from the substrate should have the same form:

$$I^e(r) = I_0^e e^{-r^2/2\sigma^2} \tag{I.3}$$

where $I_0^e$ is the corresponding amplitude of the photogenerated electron intensity. The number of fluorine atoms in the sample at any time, $t$, and position, $r$, is given for a first-order process by

$$N_F(r,t) = N_0 e^{-\gamma I^e(r)t} = N_0 \exp(-\gamma I_0^e t e^{-r^2/2\sigma^2}) \tag{I.4}$$

where $\gamma$ is a constant of proportionality in the first-order rate equation. Now, the number of F(1s) photoelectrons detected by the spectrometer per unit area, irradiated with an X-ray beam with a Gaussian spatial profile is given by

$$dI_{F(1s)}^{Gaussian}/dA = C_0 N_F(r,t)\, I^x(r) \tag{I.5}$$

where $C_0$ is a constant determined by the F(1s) photoelectron scattering cross section, the electron inelastic mean free path, the takeoff angle to the detector, the efficiency of the detector, and the étendue of the instrument.[44] Integrating this expression spatially gives the intensity of F(1s) photoelectrons detected as a function of time:

$$I_{F(1s)}^{Gaussian}(t) = \int_0^\infty N_F(r,t)\, I^x(r) C_0 2\pi r\, dr \tag{I.6}$$

$$= 2\pi I_0^x C_0 N_0 \int_0^\infty e^{-r^2/2\sigma^2} \exp(-\gamma I_0^e t e^{-r^2/2\sigma^2}) r\, dr \tag{I.7}$$

$$= 2\pi I_0^x C_0 N_0 \int_0^\infty \frac{\sigma^2}{\gamma I_0^e t} \frac{d}{dr}[\exp(-\gamma I_0^e t e^{-r^2/2\sigma^2})] \tag{I.8}$$

$$I_{F(1s)}^{Gaussian}(t) = \frac{2\pi I_0^x C_0 N_0 \sigma^2}{\gamma I_0^e t}[1 - e^{-\gamma I_0^e t}] \tag{I.9}$$

By defining the damage constant, $b$, and the initial F(1s) intensity, $I_{F(1s),t=0}$, as

$$b = \gamma I_0^e \tag{I.10}$$

$$I_{F(1s),t=0} = 2\pi I_0^x C_0 N_0 \sigma^2 \tag{I.11}$$

we can simplify eq 9:

$$I_{F(1s)}^{Gaussian}(t)/I_{F(1s),t=0} = (1 - e^{-bt})/bt \tag{I.12}$$

to yield the normalized form of the first-order decay law for the case of the Gaussian X-ray beam profile discussed under the analysis of the kinetics of loss of fluorine from SAMs.

## Appendix II. Determination of the Number of Inelastically Scattered Electrons Leading to Damage in the SAM Relative to the $Au/S(CH_2)_{11}NHCOCF_3$ System

In we noted that the damage to the SAMs occurs in a region, $\delta$, near the monolayer-vacuum interface of thickness, $\delta = 3 \pm 2$ Å. Electrons with lower kinetic energy have a smaller inelastic mean-free path in the SAM and, hence, have a greater probability of having an inelastic scattering event leading to damage. By XPS we measure the number of primary and secondary electrons at each kinetic energy in the range 130–1486 eV. The intensity of electrons having transversed the damage region, $\delta$, is given by Beer's law:

$$ne(\delta) = n_e^0 e^{-\delta/\lambda} \tag{II.1}$$

where $n_e^0$ is the intensity of electrons prior to transversing the damage region and $\lambda$ is the inelastic mean-free path.[9,46] The number of electrons inelastically scattered in this region is given by the difference

$$\Delta n_e = n_e^0 - n_e(\delta) \tag{II.2}$$

or factoring out the intensity of electrons exiting the SAM, $n_e(\delta)$, we have

$$\Delta n_e = n_e(\delta)\left[\frac{1 - e^{-\delta/\lambda}}{e^{-\delta/\lambda}}\right] \tag{II.3}$$

Expanding the number of inelastically scattered electrons in the small ratio of $\delta/\lambda$[51] gives

$$\Delta n_e \cong n_e(\delta)\left[\frac{\delta}{\lambda} + \frac{\delta^2}{2\lambda^2} + \frac{\delta^3}{6\lambda^3} + \ldots\right] \tag{II.4}$$

Keeping only the leading term and rewriting $n_e(\delta)$ in terms of kinetic energy, KE, we obtain eq 5 where $J(KE)$[43] is the intensity of electrons as measured by XPS and $G(KE)$[44] is a small correction for instrumental étendue:

$$\Delta n_e(KE) \cong \frac{\delta n_e(\delta)}{\lambda} = \frac{\delta J(KE)\, G(KE)}{\lambda(KE)} \tag{II.5}$$

Then, relative to the $Au/S(CH_2)_{11}NHCOCF_3$ system, the number

of inelastically scattered electrons in the SAM that leads to damage on any of the substrates studied is

$$N_e^{\text{inelas}}(\text{KE}) = \frac{\Delta n_e(\text{KE})}{[\Delta n_e(\text{KE})]_{\text{Au}}} = \frac{\delta J(\text{KE})\, G(\text{KE})/\lambda(\text{KE})}{(\delta J(\text{KE})\, G(\text{KE})/\lambda(\text{KE}))_{\text{Au}}} \quad \text{(II.6)}$$

Since the damage region, $\delta$, near the monolayer–vacuum interface for the trifluoroacetamido-terminated monolayers on each substrate should be the same, we can simplify this expression as

$$N_e^{\text{inelas}}(\text{KE}) = \frac{J(\text{KE})\, G(\text{KE})/\lambda(\text{KE})}{(J(\text{KE})\, G(\text{KE})/\lambda(\text{KE}))_{\text{Au}}} \quad \text{(II.7)}$$

Hence, the weighted sum over all measured kinetic energies for the number of inelastically scattered electrons in these $CF_3CONH$-terminated monolayers relative to the $Au/S(CH_2)_{11}NHCOCF_3$ system is

$$N_e^{\text{inelas}} = \frac{\sum_{\text{KE=130 eV}}^{1487} J(\text{KE})\, G(\text{KE})/\lambda(\text{KE})}{\left(\sum_{\text{KE=130 eV}}^{1487} J(\text{KE})\, G(\text{KE})/\lambda(\text{KE})\right)_{\text{Au}}} \quad \text{(II.8)}$$

as discussed under the investigation of the physical mechanism of X-ray damage to SAMS on metals.

## References and Notes


(1) Boyne, D.; Hsia, L.; Wachnik, R.; Decker, R.; Wasik, C. *Appl. Phys. Lett.* **1991**, *58*, 2687–2689.

(2) Husk, D. E.; Tarrid, C.; Benitex, E. L.; Schnatterly, S. E. *Appl. Phys. Lett.* **1991**, *59*, 2052–2054.

(3) Hsu, C. C. H., Wang, L. K., Sun, J. Y. C., Wordeman, M. R., Ning, T. H. *J. Electron. Mater.* **1990**, *19*, 721–725.

(4) Spiller, E.; Eastman, D. E.; Feder, R.; Grobman, W. D.; Gudat, W.; Topalian, J. *J. Appl. Phys.* **1976**, *47*, 5450–5459.

(5) Reichmanis, E.; Houlihan, F. M.; Nalamasu, O.; Neenan, T. X. *Chem. Mater.* **1991**, *3*, 394–407.

(6) Whitesides, G. M.; Mathias, J. P.; Seto, C. T. *Science* **1991**, *254*, 1312–1319.

(7) Bain, C. D. Ph.D. Thesis, Harvard University, Cambridge, MA, 1988.

(8) Laibinis, P. E.; Graham, R. L.; Biebuyck, H. A.; Whitesides, G. M. *Science* **1991**, *254*, 981–983.

(9) Seah, M. P.; Dench, W. A. *Surf. Interface Anal.* **1979**, *1*, 2.

(10) Powell, C. J.; Seah, M. P. *J. Vac. Sci. Technol. A* **1990**, *8*, 735–763.

(11) Primary electrons are the photoelectrons and Auger electrons generated by the impact of X-rays or electrons that are characteristic of the atom from which they emanate. Secondary electrons are electrons that have been inelastically scattered within the substrate or monolayer.

(12) Berger, S. D.; Gibson, *J. M. Appl. Phys. Lett.* **1990**, *57*, 153–155.

(13) Allee, D. R.; Broers, A. N. *Appl. Phys. Lett.* **1990**, *57*, 2271–2273.

(14) Pantano, C. G.; Madey, T. E. *Appl. Surf. Sci.* **1981**, *7*, 115–141.

(15) Clark, D. T.; Brennan, W. J. *J. Electron. Spectrosc. Relat. Phenom.* **1986**, *41*, 399–410.

(16) Mihaly, G.; Zuppiroli, L. *Philos. Mag.* **1982**, *A45*, 549–562.

(17) (a) Herrera-Fierro, P., Jones, W. R., Pepper, S. V. *J. Vac. Sci. Technol. A* **1993**, *11*, 354–367. (b) Wheeler, D. R.; Pepper, S. V. *J. Vac. Sci. Technol. A* **1990**, *8*, 4046–4056. Wheeler, D. R.; Pepper, S. V. *J. Vac. Sci. Technol.* **1982**, *20*, 226–232.

(18) Chaney, R.; Barth, G. *Fresenius Z. Anal. Chem.* **1987**, *329*, 143–146.

(19) Storp, S. *Spectrochim. Acta* **1985**, *40B*, 745–756.

(20) Laibinis, P. E.; Whitesides, G. M.; Allara, D. L.; Tao, Y.-T.; Parikh, A. N.; Nuzzo, R. G. *J. Am. Chem. Soc.* **1991**, *113*, 7152–7167.

(21) Widrig, C. A.; Alves, C. A.; Porter, M. D. *J. Am. Chem. Soc.* **1991**, *113*, 2805–2810.

(22) Chidsey, C. E. D.; Liu, G.-Y.; Rowntree, P.; Scoles, C. *J. Chem. Phys.* **1989**, *91*, 4421–4423.

(23) Strong, L.; Whitesides, G. M. *Langmuir* **1988**, *4*, 546–558.

(24) Tidswell, I. M.; Rabedeau, T. A.; Pershan, P. S.; Kosowsky, S. D.; Folkers, J. P.; Whitesides, G. M. *J. Chem. Phys.* **1991**, *95*, 2854–2861.

(25) (a) Fenter, P.; Eisenberger, P.; Liang, K. S. *Phys. Rev. Lett.* **1993**, *70*, 2447–2450. (b) Fenter, P.; Eisenberger, P.; Li, J.; Camillone, N.; Bernasek, S.; Scoles, G.; Ramanarayanan, T. A.; Liang, K. S. *Langmuir* **1991**, *7*, 2013–2016.

(26) Bain, C. D.; Troughton, E. B.; Tao, Y.-T.; Evall, J.; Whitesides, G. M.; Nuzzo, R. G. *J. Am. Chem. Soc.* **1989**, *111*, 321–335.

(27) For some recent reviews, see: Bain, C. D.; Whitesides, G. M. *Angew. Chem., Int. Ed. Engl.* **1989**, *101*, 522–528. Whitesides, G. M.; Laibinis, P. E. *Langmuir* **1990**, *6*, 87–96.

(28) This information was supplied by Surface Science Instruments.

(29) Chaney, R. *Surf. Interface Anal.* **1987**, *10*, 36–47.

(30) Laibinis, P. E.; Hickman, J. J.; Wrighton, M. S.; Whitesides, G. M. *Science* **1989**, *245*, 845.

(31) Smith, G. C.; Seah, M. P. *Surf. Interface Anal.* **1990**, *15*, 751–766.

(32) Scofield, J. H. *J. Electron Spectrosc. Relat. Phenom.* **1976**, *8*, 129–137.

(33) (a) Raaen, S.; Braaten, N. A. *Phys. Rev. B* **1990**, *42*, 9151–9154. (b) Qiu, S. L.; Pan, X.; Strongin, M.; Citrin, P. H. *Phys. Rev. B* **1987**, *36*, 1292–1295. (c) Egelhoff, W. F. *Surf. Sci. Rep.* **1987**, *6*, 253–415.

(34) The kinetic energy of the F(1s) photoelectron observed for a SAM formed from a two-component mixture of $HS(CH_2)_2(CF_2)_9CF_3$ (A) and $HS(CH_2)_{10}CH_3$ (B) with a 0.90 mole fraction of (A) is 1 eV higher than for the F(1s) photoelectron from a SAM with 0.1 mole fraction of (A) [Biebuyck, H. A.; Whitesides, G. M., unpublished results].

(35) The spatial profile of the electron beam striking the X-ray anode has been measured by Lavier Fay (Surface Science Instruments) by scanning a slit system and electron detector across the electron beam. The smallest spot sizes (nominally 150 and 300 $\mu$m in diameter) are characterized by Gaussian spatial profiles. For the larger spot sizes (nominally 600 and 1000 $\mu$m in diameter) there is a greater variation in the spatial intensity than for the smaller spots sizes (typically 2:1 from the spot center to edge). The X-ray beam spatial profiles, as measured using X-ray film or a phosphorescent material placed at the sample location where the X-ray beam is projected as an ellipse, agreed with these more quantitative electron spatial profile measurements.

(36) The introduction of the $NHCOCF_3$ groups by the one-step adsorption of $HS(CH_2)_{11}NHCOCF_3$ on gold used in this study avoids the two-step process used in our previous study[8] where $HS(CH_2)_{11}OH$ was first adsorbed on gold followed by a reaction with trifluoroacetic anhydride (TFAA) to form a $Au/S(CH_2)_{11}OCOCF_3$ system. The use of trifluoroacetic anhydride in forming a SAM on the Au dot would have also resulted in a reaction of TFAA with hydroxyl groups present on the $Si/SiO_2$ surface. The site-specific reaction of $HS(CH_2)_{11}NHCOCF_3$ with only the surface of the 350-$\mu$m gold dot is confirmed by the experiment reported in the text.

(37) The observation of contrast in these images (obtained in a scanning electron microscope) results from the different amounts of fluorine lost from the monolayer: areas appearing bright in the image represent regions with less fluorine (because of X-ray induced damage) compared to adjacent regions that are darker. The level of contrast in Figure 4 is similar to that we observed for adjacent regions in SAMs patterned with $HS(CH_2)_{11}OH$ and $HS(CH_2)_{11}NHCOCF_3$. We believe this contrast results primarily from the attenuation of low energy electrons from the gold substrate that comprise the largest part of the SEM signal. We note that these images are taken within 5 s of exposure to a weak (80 pA, 20 keV) electron beam.[38] Longer exposures of the imaged region to the electron beam results in loss of contrast in the image due to electron-induced damage of the monolayer, as we expected from our previous studies of damage to SAMs.[7,8]

(38) Lopez, G.; Biebuyck, H. A.; Whitesides, G. M. *Langmuir* **1993**, *9*, 1513–1516.

(39) The relationship between the damage constant for the case of a first-order decay with a Gaussian X-ray beam profile, $b$, and the initial damage rate constant, $k$ (shown in Table I) is $b = 2k$. This relation is easily shown from a Taylor series expansion of eq 2.

(40) Allara, D. L.; Nuzzo, R. G. *Langmuir* **1985**, *1*, 45–52.

(41) Laibinis, P. E.; Whitesides, G. M.; Allara, D. L.; Tao, Y.-T.; Parikh, A. N.; Nuzzo, R. G. *J. Am. Chem. Soc.* **1991**, *113*, 7152–7167.

(42) Based on the areas of the F(1s) peaks, formation of the $CF_3CONH$-terminated SAMs on the four substrates resulted in a variation of less than $\pm$ 10% in the number density of $CF_3CONH$ groups present at the monolayer–vacuum interface.

(43) (a) Hansen, H. S.; Tougaard, S.; Biebuyck, H. *J. Electron. Spectrosc. Relat. Phenom.* **1992**, *58*, 141–158. (b) Tougaard, S. *J. Electron. Spectrosc. Relat. Phenom.*, **1990**, *52*, 243–271.

(44) Seah, M. P. In *Practical Surface Analysis*; Briggs, D., Seah, M. P., Eds.; Wiley: Chichester, 1983.

(45) Seah, M. P.; Smith, G. C. *Surf. Interface Anal.* **1990**, *15*, 751–766.

(46) The inelastic mean free path for electrons of kinetic energies 130–1500 eV in hydrocarbons was taken as $\lambda$ (in Å) = 9.0 + 0.022 KE (in eV) from: Laibinis, P. E.; Bain, C. D.; Whitesides, G. M. *J. Phys. Chem.* **1991**, *95*, 7017–7021.

(47) Dolby, R. M. *Brit. J. Appl. Phys.* **1960**, *11*, 64–67.

(48) Folkers, J. P.; Laibinis, P. E.; Whitesides, G. M. *Langmuir* **1992**, *8*, 1330–1341.

(49) Several warnings have recently appeared concerning "piranha solution": Dobbs, D. A.; Bergman, R. G.; Theopold, K. H. *Chem. Eng. News* **1990**, *68* (17), 2. Wnuk, T. *Chem. Eng. News* **1990**, *68* (26), 2. Matlow, S. L. *Chem. Eng. News* **1990**, *68* (30), 2.

(50) Vig, O. P.; Trehan, I. R.; Kad, G. L.; Ghose, J. *Ind. J. Chem.* **1985**, *21B*, 784–786.

(51) Goldberg, R. R. *Methods of Real Analysis*; John Wiley and Sons: New York, 1976; pp 238–239.